Polyhedron 30 (2011) 142–153

Contents lists available at ScienceDirect

Polyhedron

journal homepage: www.elsevier.com/locate/poly

Synthesis, X-ray studies, spectroscopic characterization and DFT calculations of *p*-tolylimido rhenium(V) complexes bearing an imidazole-based ligand

B. Machura *, M. Wolff, I. Gryca

Department of Crystallography, Institute of Chemistry, University of Silesia, 9th Szkolna St., 40-006 Katowice, Poland

A R T I C L E I N F O

Article history:
Received 2 September 2010
Accepted 1 October 2010
Available online 20 October 2010

Keywords:
Rhenium imido complexes
2-(2-Hydroxyphenyl)-1H-benzimidazole
X-ray
Electronic structure
DFT and TDDFT calculations
NBO analysis

A B S T R A C T

Novel *p*-tolylimido rhenium(V) complexes [Re(p-$NC_6H_4CH_3$)X_2(hpb)(PPh_3)] and [Re(p-$NC_6H_4CH_3$)$(hpb)_2$(PPh_3)]X (X = Cl, Br) have been obtained in the reactions of [Re(p-$NC_6H_4CH_3$)$X_3$$(PPh_3)_2$] with 2-(2-hydroxyphenyl)-1H-benzimidazole (Hhpb). The compounds were identified by elemental analysis IR, UV–Vis spectroscopy and X-ray crystallography. The electronic structures of the complex [Re(p-$NC_6H_4CH_3$)Cl_2(hpb)(PPh_3)] and the cation $[Re(p\text{-}NC_6H_4CH_3)(hpb)_2(PPh_3)]^+$ have been calculated with the density functional theory (DFT) method. Additional information about binding in the [Re(p-$NC_6H_4CH_3$)Cl_2(hpb)(PPh_3)] and $[Re(p\text{-}NC_6H_4CH_3)(hpb)_2(PPh_3)]^+$ has been obtained by NBO analysis. The electronic spectra of [Re(p-$NC_6H_4CH_3$)Cl_2(hpb)(PPh_3)] and [Re(p-$NC_6H_4CH_3$)$(hpb)_2$(PPh_3)]Cl were investigated at the TDDFT level employing B3LYP functional in combination with LANL2DZ.

1. Introduction

Imidazole and its derivatives are an important class of heterocycle with N-donor atoms, which can be excellent organic ligands to generate various complexes upon ligation. The imidazole ring possesses two adjacent nucleophilic sites and its steric and electronic properties can be modified by the substituents of the heterocyclic ring. As a monodentate ligand it coordinates to the metal ion *via* the pyridine-type nitrogen. The pyrrole-type nitrogen (N–H) is usually involved in hydrogen bond formation with available hydrogen acceptor and/or hydrogen donor sites. In many cases these hydrogen bonds dictate interesting molecular packing and arrangements in the solid state. On the other hand, the imidazolate anion can function as a bridge ligand through both nitrogens affording polynuclear complexes of intriguing structural diversities, properties and reactivities, not found for mononuclear complexes [1–5]. Furthermore the imidazole ring is an essential metal binding site in metalloproteins, therefore complexes containing imidazole-derived ligands are important in the context of biomimetic models [6–10].

Due to the favourable nuclear properties of ^{186}Re and ^{188}Re nuclides (^{186}Re: 1.07 MeV β-emitter, $t_{1/2}$ 90 h) and ^{188}Re: 2.12 MeV β-emitter, $t_{1/2}$ 17 h) in radionuclide therapy, chemistry of oxo and imido rhenium complexes with imidazole-derived ligands arouses particular interest [11,12].

Previously, we investigated the reactivity of oxorhenium(V) species [$ReOX_3$$(EPh_3)_2$] (X = Cl or Br; E = As, P) towards 2-(2-hydroxyphenyl)-1H-benzimidazole (Hhpb). The 2-(2-hydroxyphenyl)-1H-benzimidazole has been shown to bind to rhenium(V) as a chelate, and the reactions [$ReOX_3$$(PPh_3)_2$] with Hhpb lead to the formation of *cis* and *trans* stereoisomers of [$ReOX_2$(hmbzim)(PPh_3)]. The disubstituted [ReO(OMe)$(hpb)_2$]·MeCN complex has been isolated from the reaction of [$ReOX_3$$(PPh_3)_2$] with ligand excess in a mixture of acetonitrile and methanol [13].

As an extension of this work, we decided to examine the reactivity of the related imido complexes [Re(p-$NC_6H_4CH_3$)$X_3$$(PPh_3)_2$] (X = Cl, Br) towards 2-(2-hydroxyphenyl)-1H-benzimidazole (Hhpb; Scheme 1).

The complexes containing NR^{2-} ligand have this advantage over oxocomplexes that the incorporation of functional groups in the organic moiety R may facilitate the linking of the rhenium(V) imido complex to biologically relevant molecules. In addition, the incorporation of the Re = N–R core would allow the modification of the organic substituent R to manipulate the biodistribution of the radiopharmaceutical.

Here we present the structural and spectral properties of *trans*-[Re(p-$NC_6H_4CH_3$)X_2(hpb)(PPh_3)] and [Re(p-$NC_6H_4CH_3$)$(hpb)_2$(PPh_3)]X (X = Cl, Br). The experimental studies on the imido rhenium complexes have been accompanied computationally by the density functional theory (DFT) and time-dependent DFT calculations [14,15]. Additional information about bonding between the rhenium atom and imido ligand in *trans*-[Re(p-$NC_6H_4CH_3$)Cl_2(hpb)(PPh_3)] and $[Re(p\text{-}NC_6H_4CH_3)(hpb)_2(PPh_3)]^+$ has been obtained by NBO analysis.

---

* Corresponding author.
E-mail address: basia@ich.us.edu.pl (B. Machura).

0277-5387/$ - see front matter © 2010 Elsevier Ltd. All rights reserved.
doi:10.1016/j.poly.2010.10.002

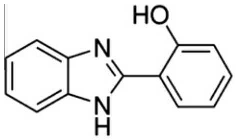

Scheme 1. Structure of Hhpb ligand.

2. Experimental

2.1. General procedure

All the reagents used to the synthesis were commercially available and were used without further purification. The complexes [Re(p-$NC_6H_4CH_3$)X_3(PPh_3)$_2$] (X = Cl, Br) were prepared according to the literature methods [16].

IR spectra were recorded on a Nicolet Magna 560 spectrophotometer in the spectral range 4000–400 cm^{-1} with the samples in form of KBr pellets. Electronic spectra were measured on a spectrophotometer Lab Alliance UV–Vis 8500 in the range 1100–180 nm. Elemental analyses (C, H, N) were performed on a Perkin–Elmer CHN-2400 analyzer. ^1H NMR spectrum was obtained in DMSO-d_6 using Bruker Avance 400 spectrometer.

2.2. Preparation of [Re(p-$NC_6H_4CH_3$)Cl_2(hpb)(PPh_3)] (**1**)

[Re(p-$NC_6H_4CH_3$)Cl_3(PPh_3)$_2$] (0.50 g, 0.54 mmol) was added to 2-(2-hydroxyphenyl)-1H-benzimidazole (0.12 g, 0.57 mmol) in acetonitrile (80 ml) and the reaction mixture was refluxed for 6 h. The resulting solution was reduced in volume to ~10 ml and allowed to cool to room temperature. A green crystalline precipitate was filtered off and dried in the air. Yield 80%. X-ray quality crystals of *trans*-[Re(p-$NC_6H_4CH_3$)Cl_2(hpb)(PPh_3)] were obtained by slow recrystallization from an acetonitrile.

Anal. Calc. for $C_{38}H_3Cl_2N_3OPRe$: C, 54.74; H, 3.75; N, 5.04. Found: C, 54.55; H, 3.67; N, 5.15%. ^1H NMR (400 MHz; DMSO-d_6) δ = 13.82 (1H, N–H), 8.04 (d, 1H), 7.65 (d, 1H), 7.53 (t, 1H), 7.42–7.32 (m, 8H), 7.28–7.18 (m, 4H), 7.14 (d, 1H), 7.07 (t, 1H), 7.03–6.90 (m, 4H), 6.84 (d, 1H), 6.73 (t, 1H), 6.65 (d, 1H), 6.51 (t, 1H), 6.83 (d, 1H), 5.59 (d, 1H), 2.14 (s, 3H).

2.3. Preparation of [Re(p-$NC_6H_4CH_3$)Br_2(hpb)(PPh_3)] (**2**)

A procedure similar to that for **1** was used with [Re(p-$NC_6H_4CH_3$)Br_3(PPh_3)$_2$] (0.50 g, 0.47 mmol) and Hhpb (0.11 g, 0.52 mmol). Green crystals of **2** were collected in 75%.

Anal. Calc. for $C_{38}H_3Br_2N_3OPRe$: C, 49.47; H, 3.39; N, 4.55. Found: C, 49.68; H, 3.29; N, 4.49%.

^1H NMR (400 MHz; DMSO-d_6) δ = 13.71 (1H, N–H), 8.06 (d, 1H), 7.83–7.72 (m, 5H), 7.69–7.52 (m, 4H), 7.51–7.41 (m, 7H), 7.36 (d, 1H), 7.30 (t, 1H), 7.18 (t, 2H), 7.12 (d, 2H), 7.09 (t, 2H), 6.96 (t, 1H), 5.99(d, 1H), 2.121 (s, 3H). UV–Vis of **2** (CH_3CN; λ_{max} [nm] (ε; [$dm^3\ mol^{-1}\ cm^{-1}$]): 675.2 (290), 326.8 (13600), 297.8 (17900), 206.8 (70050).

2.4. Preparation of [Re(p-$NC_6H_4CH_3$)(hpb)$_2$(PPh_3)]Cl (**3**)

[Re(p-$NC_6H_4CH_3$)Cl_3(PPh_3)$_2$] (0.50 g, 0.54 mmol) was added to 2-(2-hydroxyphenyl)-1H-benzimidazole (0.50 g, 2.38 mmol) in methanol (80 ml) and the reaction mixture was refluxed for 12 h. The resulting solution was reduced in volume to ~10 ml and allowed to cool to room temperature. Green crystalline precipitate was filtered off and dried in the air. Yield 70%. X-ray quality crystals of [Re(p-$NC_6H_4CH_3$)(hpb)$_2$(PPh_3)]Cl were obtained by slow recrystallization from methanol.

Anal. Calc. for $C_{51}H_{40}N_5O_2PClRe$: C, 60.80; H, 4.00; N, 6.95. Found: C, 60.46; H, 3.92; N, 6.89%.

Table 1
Crystal data and structure refinement for **1**, **2**, **3** and **4**.

	1	2	3	4
Empirical formula	$C_{38}H_{31}Cl_2N_3OPRe$	$C_{38}H_{31}Br_2N_3OPRe$	$C_{51}H_{40}N_5O_2PClRe$	$C_{51}H_{40}BrN_5O_2PRe$
Formula weight	833.73	922.65	1007.50	1051.96
Temperature	293.0(2)	293.0(2)	293.0(2)	293.0(2)
Wavelength (Å)	0.71073	0.71073	0.71073	0.71073
Crystal system	orthorhombic	monoclinic	orthorhombic	orthorhombic
Space group	*Pbca*	$P2_1/n$	$Pna2_1$	$Pna2_1$
Unit cell dimensions (Å), (°)				
a (Å)	11.095(2)	10.096(2)	21.254(4)	21.220(4)
b (Å)	17.170(3)	15.682(3)	10.124(2)	10.136(2)
		β = 96.71(3)°		
c (Å)	35.531(7)	21.653(4)	20.177(4)	20.196(4)
V (Å)	6769(2)	3404.6(12)	4341.3(15)	4344.0(15)
Z	8	4	4	4
D_{calc} (mg/m^3)	1.636	1.800	1.541	1.608
Absorption coefficient (mm^{-1})	3.831	5.999	2.945	3.802
F(0 0 0)	3296	1792	2016	2088
Crystal size (mm)	0.032 × 0.060 × 0.112	0.031 × 0.136 × 0.260	0.072 × 0.218 × 0.520	0.157×0.288 × 0.588
θ Range for data collection (°)	3.30–25.00	3.50	3.51–25.00	3.43–25.05
Index ranges	$-13 \leqslant h \leqslant 13$	$-12 \leqslant h \leqslant 12$	$-25 \leqslant h \leqslant 22$	$-25 \leqslant h \leqslant 25$
	$-20 \leqslant k \leqslant 20$	$-18 \leqslant k \leqslant 18$	$-12 \leqslant k \leqslant 11$	$-12 \leqslant k \leqslant 12$
	$-42 \leqslant l \leqslant 38$	$-25 \leqslant l \leqslant 24$	$-23 \leqslant l \leqslant 18$	$-24 \leqslant l \leqslant 23$
Reflections collected	34541	31635	19985	20767
Independent reflections	5949 (R_{int} = 0.0404)	5965 (R_{int} = 0.0492)	6794 (R_{int} = 0.0528)	7572 (R_{int} = 0.0403)
Completeness to 2θ = 25°	99.8%	99.7%	99.7%	99.6%
Minimum and maximum transmission	0.546 and 1.000	0.126 and 1.000	0.316 and 1.000	0.426 and 1.000
Data/restraints/parameters	5949/0/416	5965/0/416	6794/1/551	7572/1/551
Goodness-of-fit on F^2	1.066	1.037	1.021	1.015
Final *R* indices [$I > 2\sigma(I)$]	R_1 = 0.0285	R_1 = 0.0314	R_1 = 0.0376	R_1 = 0.0405
	wR_2 = 0.0488	wR_2 = 0.0583	wR_2 = 0.0961	wR_2 = 0.1212
R indices (all data)	R_1 = 0.0442	R_1 = 0.0526	R_1 = 0.0482	R_1 = 0.0475
	wR_2 = 0.0515	wR_2 = 0.0630	wR_2 = 0.1000	wR_2 = 0.1237
Absolute structure parameter			0.018(9)	0.006(10)
Largest difference in peak and hole [e Å^{-3}]	0.581 and −1.255	0.872 and −0.718	1.494 and −1.060	0.923 and −2.292

[*] H.D. Flack, Acta Crystallogr., Sect. A 39 (1983) 876.

^{1}H NMR (400 MHz; DMSO-d_6) δ = 13.70 (2H, N–H), 8.07 (t, 3H), 7.85–7.70(m, 9H), 7.51–7.41 (m, 14H), 7.40–7.28 (m, 2H), 7.22–7.04 (m, 5H), 6.96 (t, 1H), 5.98 (d, 1H), 2.21 (s, 3H).

2.5. Preparation of [Re(p-$NC_6H_4CH_3$)(hpb)$_2$(PPh_3)]Br (**4**)

A procedure similar to that for **3** was used with [Re(p-$NC_6H_4CH_3$)Br_3(PPh_3)$_2$] (0.50 g, 0.47 mmol) and Hhpb (0.50 g, 2.38 mmol). Green crystals of **2** were collected in 75%.

Anal. Calc. for $C_{51}H_{40}N_5O_2PBrRe$: C, 58.23; H, 3.83; N, 6.66. Found: C, 58.39; H, 3.76; N, 6.74%. ^{1}H NMR (400 MHz; DMSO-d_6) δ = 13.72 (2H, N–H), 8.07 (t, 3H), 7.90–7.70(m, 9H), 7.71–7.43 (m, 14H), 7.41–7.27 (m, 2H), 7.27–7.00 (m, 5H), 6.96 (t, 1H), 5.98 (d, 1H), 2.21 (s, 3H).

UV–Vis of **4** (CH_3CN; λ_{max} [nm] (ε; [$dm^3\ mol^{-1}\ cm^{-1}$]): 604.2 (515), 370.0 (2270), 313.0 (2125), 295.0 (8920), 202.2 (38150).

2.6. Crystal structures determination and refinement

The X-ray intensity data of **1**, **2**, **3** and **4** were collected on a Gemini A Ultra diffractometer equipped with Atlas CCD detector and graphite monochromated Mo Kα radiation (λ = 0.71073 Å) at room temperature. Details concerning crystal data and refinement are given in Table 1. Lorentz, polarization and empirical absorption correction using spherical harmonics implemented in SCALE3 ABSPACK scaling algorithm [17] were applied. The structures were solved by the Patterson method and subsequently completed by the difference Fourier recycling. All the non-hydrogen atoms were refined anisotropically using full-matrix, least-squares technique. The hydrogen atoms were treated as "riding" on their parent carbon atoms and assigned isotropic temperature factors equal 1.2 (non-methyl) and 1.5 (methyl) times the value of equivalent temperature factor of the parent atom. The methyl groups were allowed to rotate about their local threefold axis. SHELXS97 and SHELXL97 [18] programs were used for all the calculations. Atomic scattering factors were those incorporated in the computer programs.

3. Computational details

The gas phase ground state geometries of [Re(p-$NC_6H_4CH_3$)Cl_2(hpb)(PPh_3)] and [Re(p-$NC_6H_4CH_3$)(hpb)$_2$(PPh_3)]$^+$ were optimized in a closed-shell singlet (S = 1) states without any symmetry restrictions with the DFT method using the hybrid B3LYP functional of GAUSSIAN-03 [19–21]. The calculations were performed using ECP LANL2DZ basis set [22] with an additional d and f function with the exponent α = 0.3811 and α = 2.033 [23] for rhenium and the standard 6-31G basis set for other atoms. For chlorine, oxygen, nitrogen and phosphorous atoms, diffuse and polarization functions were added [24–29]. All vibrations in the calculated vibrational spectra of [Re(p-$NC_6H_4CH_3$)Cl_2(hpb)(PPh_3)] and [Re(p-$NC_6H_4CH_3$)(hpb)$_2$(PPh_3)]$^+$ were real thus the geometries correspond to true energy minima.

The electronic spectra of [Re(p-$NC_6H_4CH_3$)Cl_2(hpb)(PPh_3)] and [Re(p-$NC_6H_4CH_3$)(hpb)$_2$(PPh_3)]$^+$ were calculated with the TDDFT method [30], and the solvent effect was simulated using the polarizable continuum model with the integral equation formalism (IEF-PCM) [31–34].

Natural bond orbital (NBO) calculations were performed with the NBO code [35] included in Gaussian03.

4. Results and discussion

4.1. Preparation

The imido complexes [Re(p-$NC_6H_4CH_3$)X_2(hpb)(PPh_3)] (X = Cl, Br) were prepared in good yield by a route analogous to that used for the synthesis of the [$ReOX_2$(hpb)(PPh_3)$_2$], namely by ligand exchange reactions starting from the [Re(p-$NC_6H_4CH_3$)X_3(PPh_3)$_2$] complexes and 2-(2-hydroxyphenyl)-1H-benzimidazole (Hhpb) in molar ratio 1:1: the disubstituted imido compounds [Re(p-$NC_6H_4CH_3$)(hpb)$_2$(PPh_3)]X have been isolated from the reactions of [Re(p-$NC_6H_4CH_3$)X_2(hpb)(PPh_3)] with an excess of Hhpb in methanol (Scheme 2). Similar to the related oxocompounds methanol favour formation of the disubstituted complexes.

As the imido core NR^{2-} is isoelectronic to the $O^{2-\cdot}$ moiety, a short comparison with the Re(V) oxocompounds deserves comment. The complexes [Re(p-$NC_6H_4CH_3$)X_3(PPh_3)$_2$] are related to the oxocompounds [$ReOX_3$(PPh_3)$_2$], which have proven to be useful precursors in the synthesis of Re(V) oxocompounds incorporating N,O-donor chelate ligands [13,36–39]. Our studies have shown that the [Re(p-$NC_6H_4CH_3$)X_3(PPh_3)$_2$] compounds easily react with 2-(2-hydroxyphenyl)-1H-benzimidazole to give monosubstituted [Re(p-$NC_6H_4CH_3$)X_2(hpb)(PPh_3)] complexes with *trans-X,X*

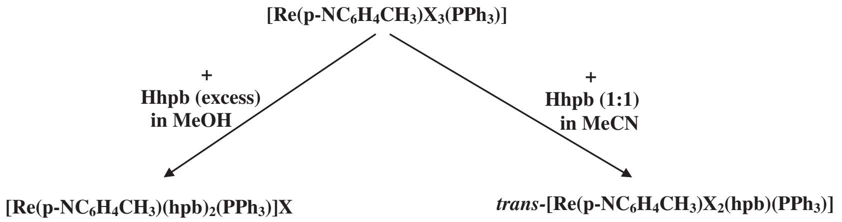

Scheme 2.

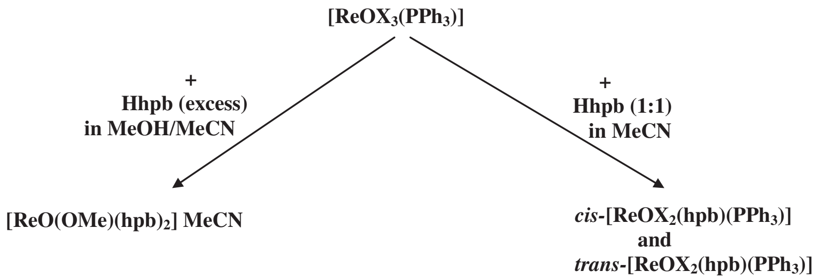

Scheme 3.

arrangement of the halide ions and disubstituted [Re(p-$NC_6H_4CH_3$)(hpb)$_2$(PPh_3)]X compounds. This contrasts with the exchange reactions performed with oxocompounds [$ReOX_3(PPh_3)_2$]. The reactions of [$ReOX_3(PPh_3)_2$] with 2-(2-hydroxyphenyl)-1H-benzimidazole in molar ratio 1:1 yield a mixture of *cis* and *trans* stereoisomers of [$ReOX_2$(hpb)(PPh_3)], whereas the reactions of [$ReOX_3(PPh_3)_2$] with an excess 2-(2-hydroxyphenyl)-1H-benzimidazole lead to [ReO(OMe)(hpb)$_2$]·MeCN [13] (Scheme 3).

The majority of the known [$ReOX_2$(O–N)(PPh_3)] structures has halide ligands in *cis* geometry. The *trans-X,X* conformation is far more rarely in this type of complexes, and it has been previously confirmed for [$ReCl_2$(APO)(PPh_3)] and [$ReOCl_2$(DPO)(PPh_3)]-(APOH = 4-anilino-3-penten-2-one; DPOH = 4-[2,6-dimethylanilino]-3-penten-2-one) [39]. A mixture of *cis* and *trans* stereoisomers [$ReOX_2$(N–O)(PPh_3)] was also isolated from the reactions of [$ReOX_3(PPh_3)_2$] with 2-(2′-hydroxyphenyl)-2-benzothiazole, but *cis*-halide isomer [$ReOX_2$(N–O)(PPh_3)] was a main product in these reactions [38]. The imido rhenium complexes incorporating uninegative N,O-donor chelate ligands have been studied rarely [40,41]. However, the *trans-X,X* arrangement of halide ions seems to be favoured in the [Re(NAr)X_2(N–O)(PPh_3)] compounds, probably due to presence of more bulky imido ligand.

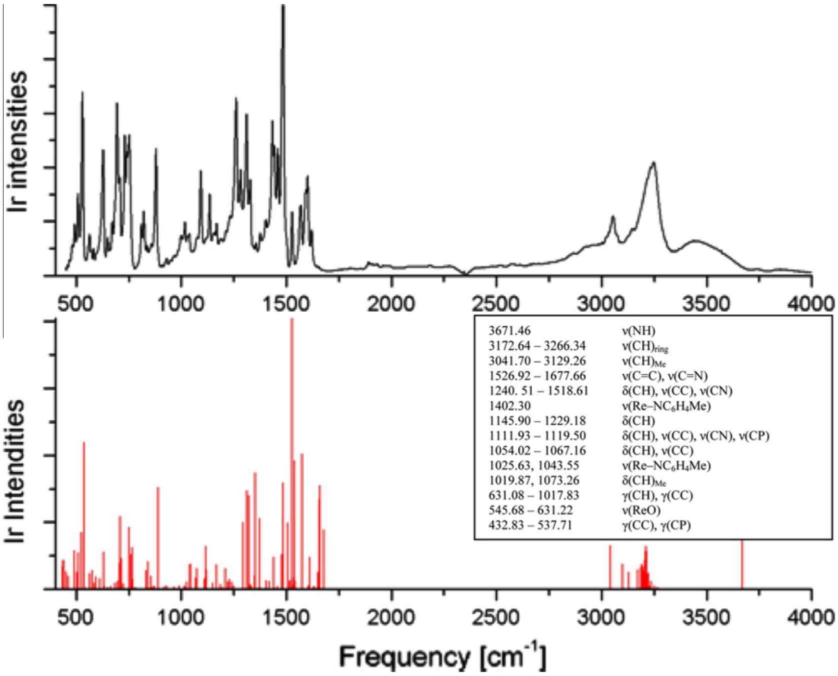

3671.46	$\nu(NH)$
3172.64 – 3266.34	$\nu(CH)_{ring}$
3041.70 – 3129.26	$\nu(CH)_{Me}$
1526.92 – 1677.66	$\nu(C{=}C)$, $\nu(C{=}N)$
1240. 51 – 1518.61	$\delta(CH)$, $\nu(CC)$, $\nu(CN)$
1402.30	$\nu(Re–NC_6H_4Me)$
1145.90 – 1229.18	$\delta(CH)$
1111.93 – 1119.50	$\delta(CH)$, $\nu(CC)$, $\nu(CN)$, $\nu(CP)$
1054.02 – 1067.16	$\delta(CH)$, $\nu(CC)$
1025.63, 1043.55	$\nu(Re–NC_6H_4Me)$
1019.87, 1073.26	$\delta(CH)_{Me}$
631.08 – 1017.83	$\gamma(CH)$, $\gamma(CC)$
545.68 – 631.22	$\nu(ReO)$
432.83 – 537.71	$\gamma(CC)$, $\gamma(CP)$

Fig. 1. The experimental and calculated (non-scaled) vibrational spectra of **1**.

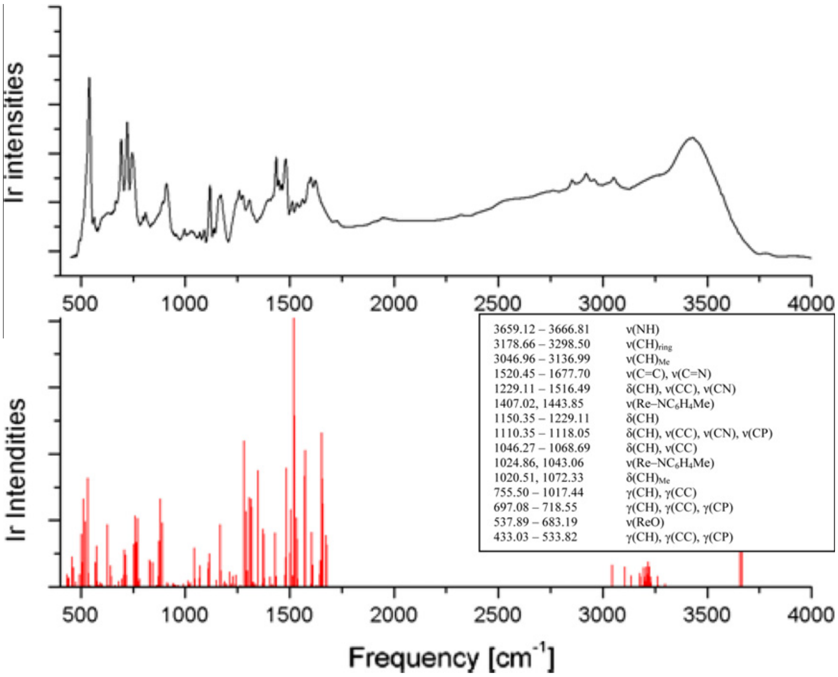

3659.12 – 3666.81	$\nu(NH)$
3178.66 – 3298.50	$\nu(CH)_{ring}$
3046.96 – 3136.99	$\nu(CH)_{Me}$
1520.45 – 1677.70	$\nu(C{=}C)$, $\nu(C{=}N)$
1229.11 – 1516.49	$\delta(CH)$, $\nu(CC)$, $\nu(CN)$
1407.02, 1443.85	$\nu(Re–NC_6H_4Me)$
1150.35 – 1229.11	$\delta(CH)$
1110.35 – 1118.05	$\delta(CH)$, $\nu(CC)$, $\nu(CN)$, $\nu(CP)$
1046.27 – 1068.69	$\delta(CH)$, $\nu(CC)$
1024.86, 1043.06	$\nu(Re–NC_6H_4Me)$
1020.51, 1072.33	$\delta(CH)_{Me}$
755.50 – 1017.44	$\gamma(CH)$, $\gamma(CC)$
697.08 – 718.55	$\gamma(CH)$, $\gamma(CC)$, $\gamma(CP)$
537.89 – 683.19	$\nu(ReO)$
433.03 – 533.82	$\gamma(CH)$, $\gamma(CC)$, $\gamma(CP)$

Fig. 2. The experimental and calculated (non-scaled) vibrational spectra of **3**.

Table 2
Short intra- and intermolecular contacts detected in **1**, **2**, **3** and **4** complexes.

D–H···A	D–H [Å]	H···A [Å]	D···A [Å]	D–H···A [°]
1				
N(3)–H(3N)···Cl(2)_$1	0.86	2.41	3.177(3)	149.2
C(2)–H(2)···Cl(2)	0.93	2.63	3.354(4)	135.1
C(16)–H(16)···Cl(1)_$2	0.93	2.83	3.499(5)	130.2
2				
N(3)–H(3N)···Br(1)#3	0.86	2.59	3.370(4)	150.8
C(27)–H(27)···N(1)	0.93	2.48	3.204(7)	134.2
C(38)–H(38)···N(3)	0.93	2.59	2.899(7)	100.2
3				
N(3)–H(3N)···Cl(1)_$4	0.86	2.29	3.092(7)	156.2
N(5)–H(5N)···Cl(1)	0.86	2.23	3.039(7)	156.2
C(8)–H(8)···O(1)	0.93	2.43	3.000(10)	119.6
C(8)–H(8)···O(2)	0.93	2.52	3.254(10)	135.8
C(17)–H(17)···Cl(1)_$5	0.93	2.73	3.590(10)	154.4
C(27)–H(27)···N(4)	0.93	2.48	3.089(10)	123.3
C(38)–H(38)···N(3)	0.93	2.55	2.862(12)	99.9
C(40)–H(40)···N(1)	0.93	2.52	3.133(11)	123.7
C(51)–H(51)···N(5)	0.93	2.62	2.919(11)	99.6
4				
N(3)–H(3N)···Br(1)_$6	0.86	2.27	3.073(7)	155.9
N(5)–H(5N)···Br(1)	0.86	2.23	3.024(8)	153.6
C(11)–H(11)···Br(1)_$7	0.93	2.71	3.578(11)	156.3
C(14)–H(14)···O(1)	0.93	2.41	2.992(11)	120.3
C(14)–H(14)···O(2)	0.93	2.52	3.256(11)	135.8
C(27)–H(27)···N(4)	0.93	2.51	3.092(11)	120.6
C(40)–H(40)···N(1)	0.93	2.53	3.134(12)	123.2
C(51)–H(51)···N(5)	0.93	2.58	2.889(12)	100.1

Symmetry transformations used to generate equivalent atoms: #1: $1 - x, -y, -z$; #2: $1/2 - x, -1/2 + y, z$; #3: $1 - x, -y, 2 - z$; #4: $-1/2 + x, 1/2 - y, z$; #5: $1 - x, -y, -1/2 + z$; #6: $-1/2 + x, 3/2 - y, z$; #7: $1 - x, 2 - y, -1/2 + z$.

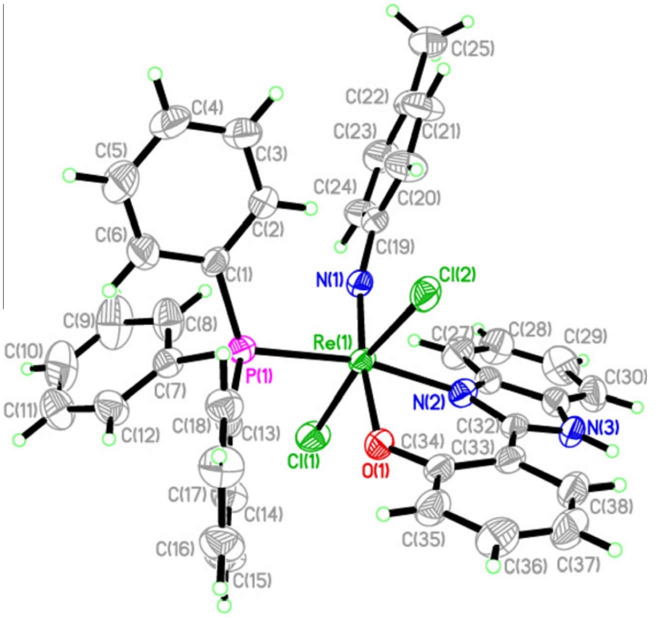

Fig. 3. The molecular structure of **1**. Displacement ellipsoids are drawn at 50% probability.

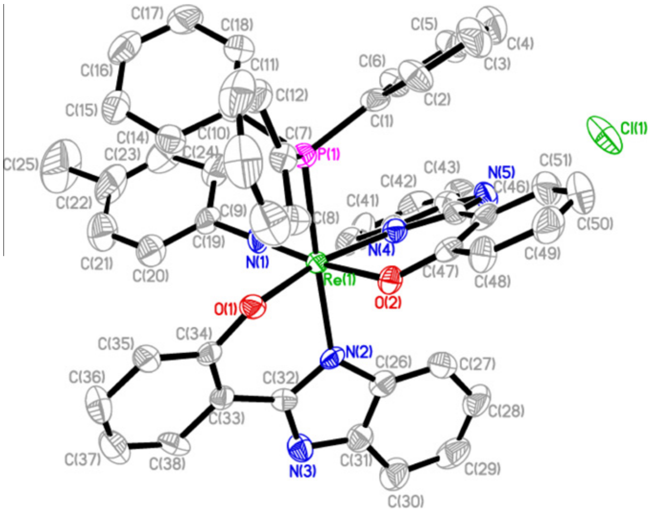

Fig. 4. The molecular structure of **3**. Displacement ellipsoids are drawn at 50% probability. Hydrogen atoms are omitted for clarity.

4.2. IR spectra and ^{1}H NMR

Characteristic bands corresponding to the ν(CN), ν(C=C) modes of the *hpb*$^-$ ligand appear in the range 1630–1530 cm^{-1}, and a band in the range 3450–3200 cm^{-1} confirms the presence N–H group in the coordinated *hpb*$^-$ ligand of the examined complexes [42]. Similar to the other related imido complexes it is extremely difficult to identify the Re-NC$_6$H$_4$CH$_3$ stretches in the IR spectra of **1**, **2**, **3** and **4**, as they may be mixed with $\nu_{C=N}$ and ν_{P-C} modes of PPh$_3$ and hpb$^-$ ligands [43–50].

The experimental vibrational spectra of **1** and **3** are compared to the calculated (non-scaled) ones (Figs. 1 and 2). The calculated ν(Re-NC$_6$H$_4$CH$_3$) frequencies appear at 1402, 1044 and 1026 cm^{-1} for **1** and 1407, 1043 and 1024 cm^{-1} for **3**.

In the ^{1}H NMR spectra of **1**, **2**, **3** and **4** the region containing signals from aromatic protons of triphenylphosphine, p-tolylimido and *hpb*$^-$ ligands (8.10–5.50 ppm) is accompanied by distinctive signals corresponding the alkyl protons of the p-tolylimido ion (2.25–2.10 ppm) and N–H protons (13.85–13.65 ppm). Owing to the overlapping of the signals of the aromatic protons of the triphenylphosphine, p-tolylimido and *hpb*$^-$, the aromatic region of the ^{1}H NMR spectra of **1**, **2**, **3** and **4** is difficult to identify.

The lack of paramagnetic broadening or shifts of resonances in the ^{1}H NMR spectra of [Re(p-NC$_6$H$_4$CH$_3$)X$_2$(hpb)(PPh$_3$)] and [Re(p-NC$_6$H$_4$CH$_3$)(hpb)$_2$(PPh$_3$)]X·(X = Cl, Br) confirms diamagnetism of the complexes.

4.3. Crystal structures

The crystallographic data of **1**, **2**, **3** and **4** are summarized in Table 1. The intra- and intermolecular contacts detected in the **1**, **2**, **3** and **4** are listed in Table 2. In all the structures the pyrrole-type nitrogen (N–H) is involved in hydrogen bond formation. The medium strength N–H···X hydrogen bonds of **1** and **2** links complex molecules into dimers, whereas the complex molecules of **3** and **4** are linked into *zig-zag* chains by N–H···X hydrogen bonds. Additionally, in all the structures exist short C–H···O, C–H···N and C–H···X interactions, which can be considered as weak or very weak hydrogen bonds [51,52].

The molecular structures of **1** and **3** are shown in Figs. 3 and 4, respectively. The selected bond lengths and angles of **1**, **2**, **3** and **4** are collected in Tables 3–6.

4.4. [Re(p-NC$_6$H$_4$CH$_3$)X$_2$(hpb)(PPh$_3$)] complexes

The complexes [Re(p-NC$_6$H$_4$CH$_3$)X$_2$(hpb)(PPh$_3$)] (X = Cl, Br) show octahedral geometry about the central rhenium atom defined by the p-methylphenylimido group, two halide ions, the phosphorus atom of PPh$_3$ molecule, and the bidentate N,O atom donors of the *hpb*$^-$ ligand. The ligands *cis* to the p-methylphenylimido group are bowed slightly away from p-NC$_6$H$_4$CH$_3$ moiety

Table 3
The experimental and optimized bond lengths (Å) and angles (°) for **1**.

Bond lengths	Experimental	Optimized	Bond angles	Experimental	Optimized
Re(1)–N(1)	1.731(3)	1.733	N(1)–Re(1)–O(1)	169.34(13)	170.18
Re(1)–O(1)	1.970(3)	2.008	N(1)–Re(1)–N(2)	95.81(13)	101.01
Re(1)–N(2)	2.145(3)	2.139	O(1)–Re(1)–N(2)	80.80(11)	81.71
Re(1)–Cl(1)	2.3747(10)	2.472	N(1)–Re(1)–Cl(1)	100.12(11)	100.33
Re(1)–P(1)	2.4477(11)	2.508	O(1)–Re(1)–Cl(1)	89.90(8)	89.22
Re(1)–Cl(2)	2.4747(10)	2.521	N(2)–Re(1)–Cl(1)	87.96(9)	86.61
			N(1)–Re(1)–P(1)	96.79(11)	91.87
			O(1)–Re(1)–P(1)	87.13(8)	85.79
			N(2)–Re(1)–P(1)	167.26(8)	167.07
			Cl(1)–Re(1)–P(1)	87.94(4)	89.95
			N(1)–Re(1)–Cl(2)	88.91(11)	88.36
			O(1)–Re(1)–Cl(2)	80.92(8)	82.43
			N(2)–Re(1)–Cl(2)	88.29(9)	85.27
			Cl(1)–Re(1)–Cl(2)	170.53(4)	169.10
			P(1)–Re(1)–Cl(2)	93.87(4)	96.38
			Re(1)–N(1)–C(19)	164.6(3)	166.30

Table 4
The experimental bond lengths (Å) and angles (°) for **2**.

Bond lengths	Experimental	Bond angles	Experimental
Re(1)–N(1)	1.713(4)	N(1)–Re(1)–O(1)	173.37(15)
Re(1)–O(1)	1.968(3)	N(1)–Re(1)–N(2)	103.65(15)
Re(1)–N(2)	2.146(4)	O(1)–Re(1)–N(2)	82.11(14)
Re(1)–P(1)	2.4408(12)	N(1)–Re(1)–P(1)	89.07(12)
Re(1)–Br(2)	2.5696(9)	O(1)–Re(1)–P(1)	85.30(10)
Re(1)–Br(1)	2.5782(9)	N(2)–Re(1)–P(1)	167.12(11)
		N(1)–Re(1)–Br(2)	90.86(13)
		O(1)–Re(1)–Br(2)	86.26(13)
		N(2)–Re(1)–Br(2)	85.89(12)
		P(1)–Re(1)–Br(2)	96.05(4)
		N(1)–Re(1)–Br(1)	95.32(13)
		O(1)–Re(1)–Br(1)	88.29(13)
		N(2)–Re(1)–Br(1)	85.82(12)
		P(1)–Re(1)–Br(1)	91.08(4)
		Br(2)–Re(1)–Br(1)	170.64(2)
		Re(1)–N(1)–C(19)	174.30(34)

Table 5
The selected experimental and optimized bond lengths (Å) and angles (°) for **3**.

Bond lengths	Experimental	Optimized	Bond angles	Experimental	Optimized
Re(1)–N(1)	1.742(6)	1.733	N(1)–Re(1)–O(2)	173.8(3)	173.66
Re(1)–O(2)	1.997(5)	2.028	N(1)–Re(1)–O(1)	95.1(2)	97.05
Re(1)–O(1)	2.036(5)	2.042	O(2)–Re(1)–O(1)	86.7(2)	87.62
Re(1)–N(4)	2.121(6)	2.176	N(1)–Re(1)–N(4)	96.7(3)	94.67
Re(1)–N(2)	2.144(6)	2.161	O(2)–Re(1)–N(4)	82.0(2)	80.71
Re(1)–P(1)	2.460(2)	2.544	O(1)–Re(1)–N(4)	167.7(2)	168.28
			N(1)–Re(1)–N(2)	98.1(3)	99.72
			O(2)–Re(1)–N(2)	87.9(2)	84.89
			O(1)–Re(1)–N(2)	85.6(2)	85.30
			N(4)–Re(1)–N(2)	89.2(2)	92.55
			N(1)–Re(1)–P(1)	90.1(2)	89.67
			O(2)–Re(1)–P(1)	84.05(16)	86.44
			O(1)–Re(1)–P(1)	88.71(15)	85.24
			N(4)–Re(1)–P(1)	94.83(17)	95.04
			N(2)–Re(1)–P(1)	170.45(16)	167.42
			Re(1)–N(1)–C(19)	172.0(6)	177.34

Table 6
The experimental bond lengths (Å) and angles (°) for **4**.

Bond lengths	Experimental	Bond angles	Experimental
Re(1)–N(1)	1.735(6)	N(1)–Re(1)–O(2)	174.2(3)
Re(1)–O(2)	1.995(6)	N(1)–Re(1)–O(1)	94.7(3)
Re(1)–O(1)	2.023(6)	O(2)–Re(1)–O(1)	87.0(2)
Re(1)–N(4)	2.116(7)	N(1)–Re(1)–N(4)	96.2(3)
Re(1)–N(2)	2.138(7)	O(2)–Re(1)–N(4)	82.5(2)
Re(1)–P(1)	2.459(2)	O(1)–Re(1)–N(4)	168.6(2)
		N(1)–Re(1)–N(2)	98.8(3)
		O(2)–Re(1)–N(2)	86.9(2)
		O(1)–Re(1)–N(2)	86.4(2)
		N(4)–Re(1)–N(2)	88.7(3)
		N(1)–Re(1)–P(1)	89.8(2)
		O(2)–Re(1)–P(1)	84.66(17)
		O(1)–Re(1)–P(1)	88.17(17)
		N(4)–Re(1)–P(1)	95.18(18)
		N(2)–Re(1)–P(1)	170.13(19)
		Re(1)–N(1)–C(19)	173.3(6)

to minimize steric congestion around the rhenium atom. The halide ions of [Re(p-NC$_6$H$_4$CH$_3$)X$_2$(hpb)(PPh$_3$)] are arranged in *trans* geometry. The oxygen atom of *hbp*$^-$ chalate ligand occupies *trans* position to the 4-methylphenylimido ion, and the triphenylphosphine molecule with their π-acidity adopts *cis* position with respect to the almost linear RN$\equiv$Re–O unit. Consequently, the RN$\equiv$Re–O core with multiply bonded imido ligand is stabilized to some extent due to accessible π-donation from rhenium to triphenylphosphine molecule. The multiple bonding imido ligand and narrow bite angle of the chelating ligand contribute to clear distortions of the pseudooctahedral environment of Re center in the [Re(p-NC$_6$H$_4$CH$_3$)X$_2$(hpb)(PPh$_3$)] complexes. In **1** and **2** the Re(1) atom is displaced respectively 0.2187(9), 0.1850(10) Å from the plane formed by the two halogen, one nitrogen and one phosphorous atoms (plane A), 0.0544(1), 0.0363(12) Å from the plane formed the two halogen, one nitrogen and one oxygen atoms (plane B) and 0.0506(14), 0.0037(19) Å from the plane formed by two nitrogen, one oxygen and one phosphorous atoms (plane C). Least squares plane A is inclined at 89.00(7)°, 86.38(7)° to plane B and at 89.56(6)°, 89.29(8)°, to plane C; planes B and C are inclined at 88.19(5)°, 88.67(7)° respectively as above.

The Re(1)–N(1)–C(19) bond angle in the structures [Re(p-NC$_6$H$_4$CH$_3$)X$_2$(hpb)(PPh$_3$)] (164.6(3)° for **1** and 174.30(34)° for **2**) agrees with the linear coordination mode of the arylimido ligands, ant it reaches a smaller value for the chloride compound. The Re–N(1) bond lengths of [Re(p-NC$_6$H$_4$CH$_3$)X$_2$(hpb)(PPh$_3$)] (1.731(3) Å for **1** and 1.713(4) Å for **2**) fall in the range 1.67–1.74 Å typical of mononuclear complexes of rhenium(V) having [Re$\equiv$NR]$^{3+}$ core, and confirm the presence of a triple bond Re$\equiv$N [43–50]. The interatomic distances between the rhenium atom and the oxygen atom of *hpb*$^-$ ligand in **1** and **2** structures are somewhat shorter than an ideal single Re–O bond length (*ca.* 2.04 Å) [53], indicating small delocalization in the RN$\equiv$Re–O unit.

The Re–P and Re–Cl bond distances fall within the normal range in six-coordinate rhenium complexes [54].

4.5. [Re(p-NC$_6$H$_4$CH$_3$)(hpb)$_2$(PPh$_3$)]X complexes

The asymmetric unit of **3** and **4** contains the cation [Re(p-NC$_6$H$_4$CH$_3$)(hpb)$_2$(PPh$_3$)]$^+$ and halide ion. The cation

Table 7
Atomic charges from the Natural Population Analysis (NPA) for **1** and **3**.

Complex	1	3
Re(1)	0.785	0.517
O(1)	−0.690	−0.637
O(2)		−0.633
Cl(1)	−0.469	
Cl(2)	−0.511	
P(1)	1.413	1.502
N(1)	−0.334	−0.260
N(2)	−0.524	−0.486
N(4)		−0.495

$[Re(p\text{-}NC_6H_4CH_3)(hpb)_2(PPh_3)]^+$ has a distorted octahedral configuration with two bidentate *hbp*$^-$ ligands, p-methylphenylimido group and triphenylphosphine molecule. Likewise in **1** and **2**, the *cis*-location of PPh_3 molecule in relation to the linear $RN{\equiv}Re–O$ unit in $[Re(p\text{-}NC_6H_4CH_3)(hpb)_2(PPh_3)]^+$ is governed by electronic influence of the multiply bonded ligand, which forces the metal nonbonding *d* electrons to lie in the plane perpendicular to the $Re{\equiv}NR$ bond axis. In **3** and **4** the Re(1) atom is displaced respectively 0.0107(30), 0.0109(31) Å from the plane formed by the two oxygen and two nitrogen atoms (plane A), 0.1862(26), 0.1824(29) Å from the plane formed the two nitrogen, one phosphorous and one oxygen atoms (plane B) and 0.0375(26), 0.0360(28) Å from the plane formed by two nitrogen, one oxygen and one phosphorous atoms (plane C). Least squares plane A is

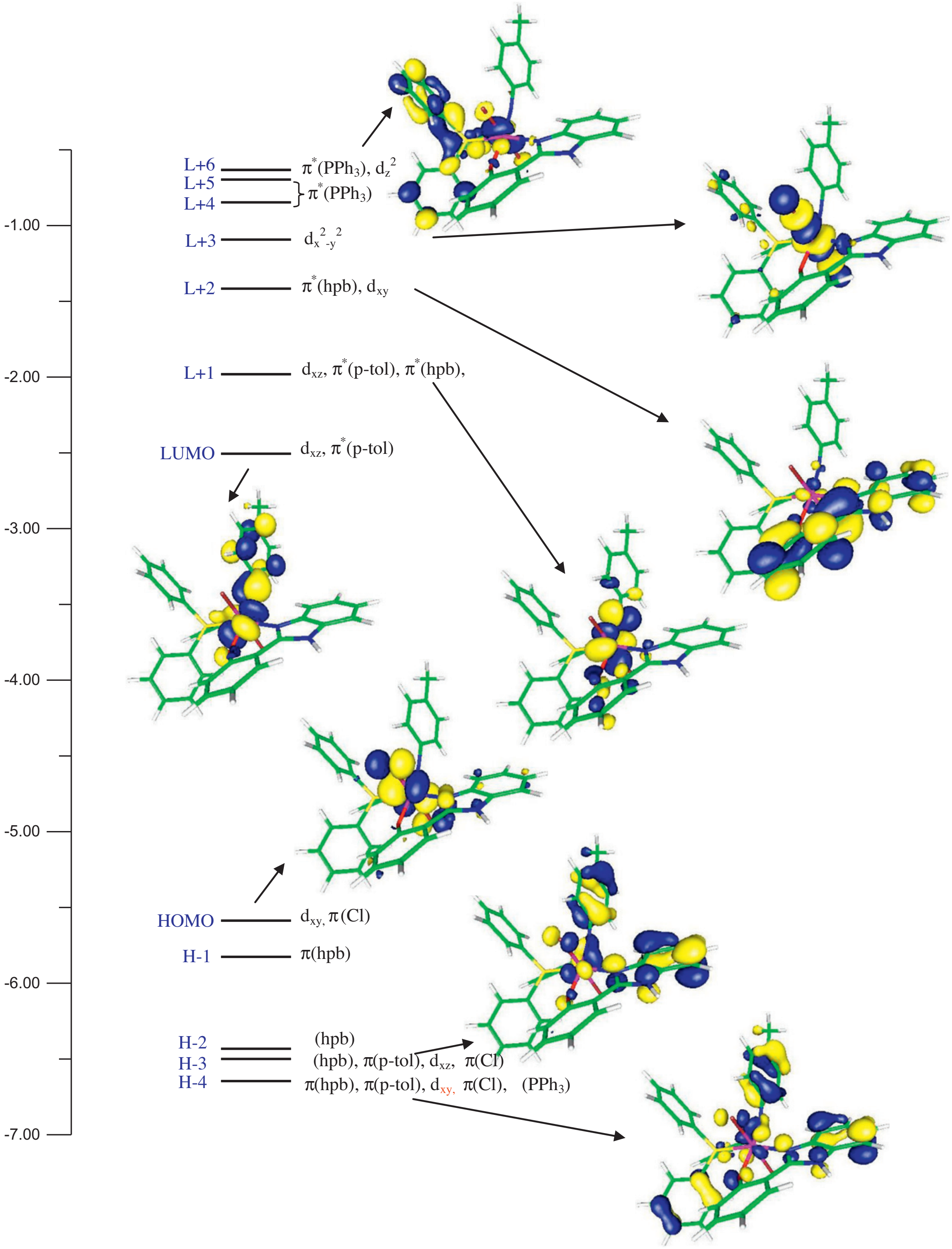

Fig. 5. The energy (eV), character and some contours of the unoccupied molecular orbitals of $[Re(p\text{-}NC_6H_4CH_3)Cl_2(hpb)(PPh_3)]$. Positive values of the orbital contour are represented in blue (0.04 au) and negative values – in yellow (−0.04 au). (For interpretation of the references to colour in this figure legend, the reader is referred to the web version of this article.)

inclined at 89.30(12)°, 88.72(13)° to plane B and at 89.10(15)°, 88.58(16)°, to plane C; planes B and C are inclined at 88.26(13)°, 88.39(14)° respectively as above.

Similar to the [Re(p-$NC_6H_4CH_3$)X_2(hpb)(PPh_3)] complexes, the Re(1)–N(1)–C(19) bond angles in the structures [Re(p-$NC_6H_4CH_3$)(hpb)$_2$(PPh_3)]X (172.0(6)° for **3** and 173.3(6)° for **4**) agree with the linear coordination mode of the arylimido ligands, and the Re–N(1) bond lengths (1.742(6) Å for **3** and 1.735(6) Å for **4**) fall in the range typical of mononuclear complexes of rhenium(V) having [Re≡NR]$^{3+}$ core [43–50].

For both complexes the interatomic distance between the rhenium atom and the oxygen atom of *hpb*$^-$ in *trans* position to the p-methylphenylimido anion is somewhat shorter than the Re–O bond in *trans* position to the benzimidazole, indicating small delocalization in the RN≡Re–O unit.

4.6. Geometry optimisations, charge distributions, electronic structures and NBO analyses

To get an insight in the electronic structures and bonding properties of the complex [Re(p-$NC_6H_4CH_3$)Cl_2(hpb)(PPh_3)] and the cation [Re(p-$NC_6H_4CH_3$)(hpb)$_2$(PPh_3)]$^+$, the calculations in the DFT method were carried out. Before the calculations of the electronic structures of the studied compounds, their geometries were optimized in singlet states using the DFT method with the B3LYP functional. The optimized geometric parameters of

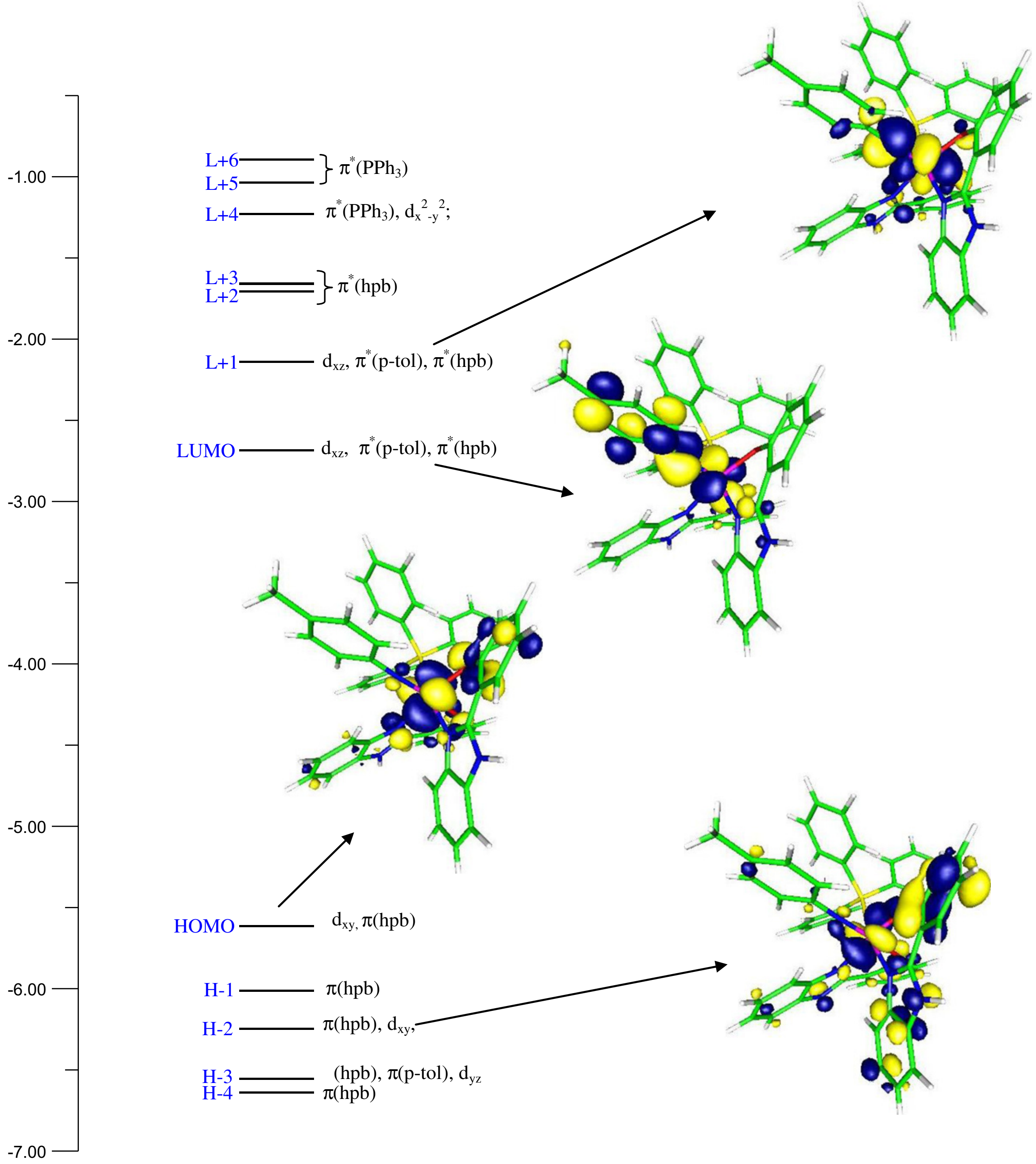

Fig. 6. The energy (eV), character and some contours of the unoccupied molecular orbitals of [Re(p-$NC_6H_4CH_3$)(hpb)$_2$(PPh_3)]$^+$. Positive values of the orbital contour are represented in blue (0.04 au) and negative values – in yellow (−0.04 au). (For interpretation of the references to colour in this figure legend, the reader is referred to the web version of this article.)

Table 8
The occupancy and composition of the calculated natural bond orbitals (NBOs) between the rhenium and the p-tolylimido ligand for [Re(p-$NC_6H_4CH_3$)Cl_2(hpb)(PPh_3)] and [Re(p-$NC_6H_4CH_3$)$(hpb)_2$(PPh_3)]$^+$.

BD	Occupancy	Composition of NBO	BD[a]	Occupancy
[Re(p-$NC_6H_4CH_3$)Cl_2(hpb)(PPh_3)]				
Re–$N_{(p\text{-tol})}$	1.96	$0.488\ (sp0.01d^{3.11})_{Re} + 0.873\ (sp^{0.81})_N$	$0.873\ (sp^{0.01}d^{3.11})_{Re} - 0.488\ (sp^{0.81})_N$	0.30
Re–$N_{(p\text{-tol})}$	1.96	$0.608\ (d)_{Re} + 0.794\ (p)_N$	$0.779\ (d)_{Re} - 0.627\ (p)_N$	0.29
Re–$N_{(p\text{-tol})}$	1.92	$0.663\ (d)_{Re} + 0.748\ (p)_N$	$0.748\ (d)_{Re} - 0.664\ (p)_N$	0.28
[Re(p-$NC_6H_4CH_3$)$(hpb)_2$(PPh_3)]$^+$				
Re–$N_{(p\text{-tol})}$	1.97	$0.623\ (d)_{Re} + 0.783\ (p)_O$	$0.783\ (d)_{Re} - 0.623\ (p)_O$	0.20
Re–$N_{(p\text{-tol})}$	1.92	$0.655\ (d)_{Re} + 0.755\ (p)_O$	$0.755\ (d)_{Re} - 0.655\ (p)_O$	0.32

BD denotes 2-center bond.
[a] Denotes antibond NBO.

Table 9
Stabilization energies associated with delocalisation from the nitrogen imido lone pair orbital of [Re(p-$NC_6H_4CH_3$)$(hpb)_2$(PPh_3)]$^+$.

Donor orbital	Occupancy of donor orbital	Acceptor orbital	ΔE_{ij} [kcal/mol]
$(sp^{1.25})_{N1}$	1.516	LP^*(2)Re1 [$(d)_{Re}$] LP^*(3)Re1 [$(sp^{0.30}d^{0.51})_{Re}$]	269.52 99.01

[Re(p-$NC_6H_4CH_3$)Cl_2(hpb)(PPh_3)] and [Re(p-$NC_6H_4CH_3$)$(hpb)_2$(PPh_3)]$^+$ are given in Tables 3 and 5. In general, the predicted bond lengths and angles are in agreement with the values based upon the X-ray crystal structure data, and the general trends observed in the experimental data are well reproduced in the calculations. The largest differences are found for the Re–Cl and Re–P bond distances. It may come from the basis sets which are approximated to a certain extent or may indicate the influence of the crystal packing on the values of the experimental bond lengths. The theoretical calculations do not consider the effects of chemical environment.

Table 7 presents the atomic charges from the Natural Population Analysis (NPA) for **1** and **3**. The calculated charge on the Re atom in the disubstituted complex is less positive in comparison with the mono-substituted one. However, the both values are considerable lower than the formal charge +5. The populations of the d_{xy}, d_{xz}, d_{yz}, $d_x^2 - y^2$ and d_z^2 rhenium orbitals are following: 1.039, 1.889, 0.951, 0.941 and 0.969 for **1** and 1.296, 1.471, 0.824, 1.070 and 0.915 for **3**. This data suggest that the donation from ligands to d_{Re} orbitals plays a key role in the electronic structure of the examined complexes. There are large positive charges on the P atoms, and the charges on the chloride and oxygen atom of *hpb*$^-$ are significantly smaller than −1.

The [Re(p-$NC_6H_4CH_3$)Cl_2(hpb)(PPh_3)] and the cation [Re(p-$NC_6H_4CH_3$)$(hpb)_2$(PPh_3)]$^+$ are closed-shell structures. Their partial molecular orbital diagrams with the several highest occupied and lowest unoccupied molecular orbital contours are presented in Figs. 5 and 6, respectively.

The highest occupied MO of [Re(p-$NC_6H_4CH_3$)Cl_2(hpb)(PPh_3)] is comprised of rhenium d_{xy} and π orbitals of chloride ions in antibonding arrangement. The remaining four d-type orbitals of rhenium are found among unoccupied MOs. It confirms d^2 configuration of the rhenium atoms in the [Re(p-$NC_6H_4CH_3$)X_2(hpb)(PPh_3)] complexes. The LUMO and LUMO + 1 are predominately localized on the rhenium atom (d_{xz} and d_{yz} orbitals) with significant contribution of the p_π nitrogen orbitals of the imido ligand. To large extent these orbitals can be ascribed as $\pi^*_{Re\equiv NR}$ orbitals. The rhenium–nitrogen interaction in **1** can be described as a triple bond. Assuming that rhenium uses its six valence orbitals, $5d_x^2 - y^2$, $5d_z^2$, 6s, $6p_x$, $6p_y$ and $6p_z$ to form σ-bonds with the six ligands, empty $5d_{xz}$ and $5d_{yz}$ orbitals are available to overlap with $2p_x$ and $2p_y$ orbitals on the imido nitrogen to form an effective triple bond as π-anti-bonding rhenium–imido

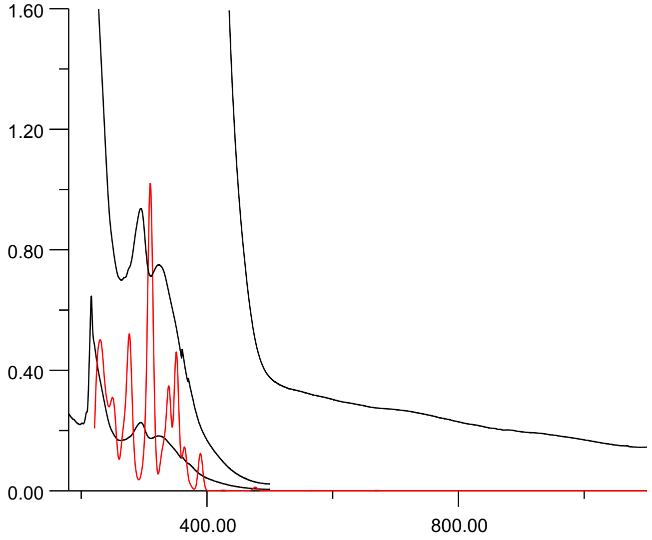

Fig. 7. The experimental (black) and calculated (red) electronic absorption spectra of **1**. (For interpretation of the references to colour in this figure legend, the reader is referred to the web version of this article.)

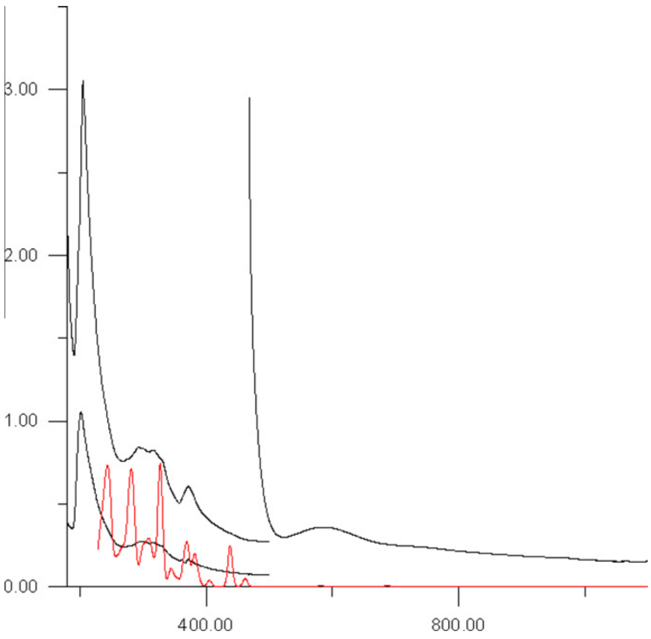

Fig. 8. The experimental (black) and calculated (red) electronic absorption spectra of **3**. (For interpretation of the references to colour in this figure legend, the reader is referred to the web version of this article.)

molecular orbitals. The $d_x^2 - y^2$ and d_z^2 rhenium orbital contributes to the LUMO + 3 and LUMO + 6, respectively. The value of the energy separation between the highest occupied molecular orbital and the lowest unoccupied molecular orbital equals to 3.09 eV.

The highest occupied MO of the cation $[Re(p\text{-}NC_6H_4CH_3)(hpb)_2(PPh_3)]^+$ is comprised of rhenium d_{xy} and π orbitals of *hpb*⁻ ligands. Similar to the monosubstituted complex, the LUMO and LUMO + 1 can be ascribed as π-anti-bonding rhenium–imido molecular orbitals. Among the lowest unoccupied MOs of$[Re(p\text{-}NC_6H_4CH_3)(hpb)_2(PPh_3)]^+$, the largest numbers constitute π orbitals of the *hpb*⁻ and PPh$_3$ligand. The $d_x^2 - y^2$ and d_z^2 rhenium orbital contributes to the higher unoccupied MO. The HOMO–LUMO gap of $[Re(p\text{-}NC_6H_4CH_3)(hpb)_2(PPh_3)]^+$ is equal to 2.93 eV.

The nature of the rhenium–imido ligand interaction in $[Re(p\text{-}NC_6H_4CH_3)Cl_2(hpb)(PPh_3)]$ and $[Re(p\text{-}NC_6H_4CH_3)(hpb)_2(PPh_3)]^+$ has been also studied by NBO analysis. The occupancy and composition of the calculated Re–NR natural bond orbitals (NBOs) are given in Table 8. Each natural bond orbital (NBO) σ_{AB} can be written in terms of two directed valence hybrids (NHOs) h_A and h_B on atoms A and B:

$$\sigma_{AB} = c_A h_A + c_A h_B \qquad (1)$$

where c_A and c_B are polarization coefficients. Each valence bonding NBO must in turn be paired with a corresponding valence antibonding NBO:

$$\sigma^*_{AB} = c_B h_A - c_A h_B \qquad (2)$$

to complete the span of the valence space. The Lewis-type (donor) NBOs are thereby complemented by the non-Lewis-type (acceptor) NBOs that are formally empty in an idealized Lewis picture. The interactions between ‘filled’ (donor) Lewis-type NBOs and ‘empty’ (acceptor) non-Lewis NBOs lead to loss of occupancy from the localized NBOs of the idealized Lewis structure into the empty non-Lewis orbitals, and they are referred to as ‘delocalization’ corrections to the zeroth-order natural Lewis structure. The stabilization energy ΔE_{ij} (kcal/mol) associated with delocalization is estimated by the second-order perturbative as:

$$\Delta E_{ij} = q_j(F(i,j)^2)/(\varepsilon_j - \varepsilon_i) \qquad (3)$$

where q_i is the donor orbital occupancy, ε_i, ε_j are diagonal elements (orbital energies) and $F(i,j)$ is the off-diagonal NBO Fock matrix element [55].

For complex $[Re(p\text{-}NC_6H_4CH_3)Cl_2(hpb)(PPh_3)]$ three Re–NR natural bond orbitals were detected. The Re–N bond orbital of σ-character is strongly polarized towards the nitrogen atom, and the s and p nitrogen orbitals and s and d rhenium orbitals take part in the bond formation. The Re–N bond orbitals of π-character are results of overlapping of the empty d_{xy} and d_{yz} rhenium orbitals with the occupied p_x and p_z orbitals of the deprotonated nitrogen of the imido ligand. For the cation $[Re(p\text{-}NC_6H_4CH_3)(hpb)_2(PPh_3)]^+$ only two Re–NR natural bond orbitals were confirmed by NBO analysis. As the detected natural Re–N bond orbitals of $[Re(p\text{-}NC_6H_4CH_3)(hpb)_2(PPh_3)]^+$ are composed of the *p* oxygen and *d* rhenium orbitals, it can be assumed that both are of π character. Not detected σ_{Re-N} bond has predominantly ionic character, similar as Re–N bond orbital in $[ReCl_4(MeCN)_2]$ [56]. Strong delocalization of the lone pair localized on the imido nitrogen atom into non-Lewis rhenium orbitals (Table 9) confirms this interpretation.

4.7. Electronic spectra

The experimental and calculated electronic spectra of **1** and **3** are presented in Figs. 7 and 8, respectively. Each calculated transition for **1** and **3** is represented by a gaussian function $y = ce^{-bx^2}$ with the height (c) equal to the oscillator strength and b equal to 0.04 nm^{-2}. The TD-DFT results obtained by using B3LYP in combination with the LANL2DZ basis set are in good agreement with the experimental spectra.

Tables 10 and 11 present the most important electronic transitions calculated with the TDDFT method assigned to the observed absorption bands of **1** and **3**, respectively. For the high energy part

Table 10
The energy and molar absorption coefficients of experimental absorption bands and the electronic transitions calculated with the TDDFT method for $[Re(p\text{-}NC_6H_4CH_3)Cl_2(hpb)(PPh_3)]$.

The most important orbital excitations	Character	λ [nm]	E [eV]	f	Experimental Λ[nm](E [eV])ε
H → L	d/π(Cl) → d/π*(p-tol)	670.2	1.85	0.0005	731.4 (1.70) 90
H → L + 1	d/π(Cl) → d/π*(p-tol)/π*(hpb)	564.6	2.20	0.0003	
H − 1 → L	π(hpb) → d/π*(p-tol)	476.7	2.60	0.0059	323.1 (3.84) 25500
H → L + 3	d/π(Cl) → d	425.8	2.91	0.0010	
H − 1 → L + 1	π(hpb) → d/π*(p-tol)/π*(hpb)	389.5	3.18	0.0619	
H − 3 → L	π(hpb)/π(p-tol)/π(Cl)/d → d/π*(p-tol)	364.2	3.40	0.0708	
H → L + 2	d/π(Cl) → π*(hpb)/d	355.3	3.49	0.0303	
H − 5 → L	π(PPh$_3$) → d/π*(p-tol)	351.8	3.52	0.0348	
H → L + 2	d/π(Cl) → π*(hpb)/d	350.7	3.54	0.1818	
H − 4 → L	π(hpb)/π(p-tol)/π(PPh$_3$)/π(Cl)/d → d/π*(p-tol)	339.7	3.65	0.1576	
H − 2 → L + 1	π(hpb) → d/π*(p-tol)/π*(hpb)	333.9	3.71	0.0496	
H − 1 → L + 2	π(hpb) → π*(hpb)/d				
H − 7 → L	π(PPh$_3$) → d/π*(p-tol)	328.3	3.78	0.0432	
H − 8 → L	π(PPh$_3$) → d/π*(p-tol)	315.3	3.93	0.0390	294.7 (4.21) 31870
H − 5 → L + 1	π(PPh$_3$) → d/π*(p-tol)/π*(hpb)	312.1	3.97	0.1506	
H − 1 → L + 3	π(hpb) → d	311.1	3.99	0.0451	
H − 2 → L + 1	π(hpb) → d/π*(p-tol)/π*(hpb)	308.7	4.02	0.3369	
H − 1 → L + 3	π(hpb) → d				
H − 12 → L	π(Cl)/π(p-tol)/π(hpb) → d/π*(p-tol)	303.7	4.08	0.0519	
H − 10 → L	π(p-tol)/π(Cl) → d/π*(p-tol)				
H − 2 → L + 2	π(hpb) → π(hpb)/d	277.2	4.47	0.1797	
H − 3 → L + 2	π(hpb)/π(p-tol)/π(Cl)/d → π*(hpb)/d	273.0	4.54	0.0516	
H − 15 → L + 1	π(Cl) → d/π*(p-tol)/π*(hpb)	247.9	5.00	0.0304	215.9 (5.74) 110110
H − 18 → L + 1	π(Cl)/π(hpb)/d → d/π*(p-tol)/π*(hpb)	230.3	5.38	0.0376	
H − 5 → L + 5	π(PPh$_3$) → π*(PPh$_3$)	229.9	5.39	0.0453	
H − 8 → L + 4	π(PPh$_3$) → π*(PPh$_3$)	225.3	5.50	0.0388	
H − 4 → L + 5	π(hpb)/π(p-tol)/π(PPh$_3$)/π(Cl)/d → π*(PPh$_3$)				

ε – molar absorption coefficient [dm^3 mol^{-1} cm^{-1}]; f – oscillator strength; H – highest occupied molecular orbital; L – lowest unoccupied molecular orbital.

Table 11
The energy and molar absorption coefficients of experimental absorption bands and the electronic transitions calculated with the TDDFT method for [Re(p-NC$_6$H$_4$CH$_3$)(hpb)$_2$(PPh$_3$)]Cl.

The most important orbital excitations	Character	λ [nm]	*E* [eV]	*f*	Experimental Λ [nm](*E* [eV])ε
H → L	d/π(hpb) → d/π*(p-tol)	687.2	1.81	0.0042	585.8 (2.12) 500
H → L + 1	d/π(hpb) → d/π*(p-tol)/π*(hpbi)	581.5	2.13	0.0047	
H – 1 → L	π(hpb) → d/π*(p-tol)	461.6	2.69	0.0249	330.8 (3.75) 5100
H – 2 → L	π(hpb)/d → d/π*(p-tol)	437.9	2.83	0.1238	
H – 1 → L + 1	π(hpb) → d/π*(p-tol)/π*(hpbi)	405.1	3.06	0.0201	
H → L + 2	d/π(hpb) → π*(hpb)	388.2	3.19	0.0213	
H → L + 3	d/π(hpb) → π*(hpb)	381.7	3.25	0.0838	
H – 3 → L	π(hpb)/π(p-tol)/d → d/π*(p-tol)	370.9	3.34	0.1065	
H – 4 → L	π(hpb) → d/π*(p-tol)	365.2	3.39	0.0765	
H – 6 → L	π(PPh$_3$)/π(hpb) → d/π*(p-tol)	344.2	3.60	0.0308	
H – 8 → L	π(p-tol)/π(PPh$_3$)/π(hpb) → d/π*(p-tol)	330.3	3.75	0.0566	315.2 (3.93) 8900
H – 1 → L + 2	π(hpb) → π*(hpb)	327.3	3.79	0.0901	
H – 1 → L + 3	π(hpb) → π*(hpb)	326.8	3.79	0.2371	
H – 2 → L + 2	d/π(hpb) → π*(hpb)	313.8	3.95	0.0308	
H – 5 → L + 1	π(hpb) → d/π*(p-tol)/π*(hpbi)	312.2	3.97	0.0422	
H – 2 → L + 2	π(hpb)/d → π*(hpb)				
H → L + 6	d/π(hpb) → π*(PPh$_3$)	309.2	4.01	0.0394	
H – 2 → L + 3	π(hpb)/d → π*(hpb)				
H – 11 → L	π(PPh$_3$) → d/π*(p-tol)	306.4	4.05	0.0376	
H – 2 → L + 3	π(hpb)/d → π*(hpb)				
H – 6 → L + 1	π(PPh$_3$)/π(hpb) → d/π*(p-tol)/π*(hpbi)	302.8	4.09	0.0343	296.8 (4.18) 9100
H – 8 → L + 1	π(p-tol)/π(PPh$_3$)/π(hpb) → d/π*(p-tol)/π*(hpbi)	298.9	4.15	0.0655	
H – 1 → L + 4	π(hpb) → π*(PPh$_3$)	294.3	4.21	0.0302	
H – 3 → L + 2	π(hpb)/π(p-tol) → π*(hpb)	285.7	4.34	0.1253	
H – 4 → L + 2	π(hpb) → π*(hpb)	282.5	4.39	0.0690	
H – 3 → L + 3	π(hpb)/π(p-tol) → π*(hpb)	280.4	4.42	0.1191	
H – 2 → L + 4	π(hpb)/d → π*(PPh$_3$)	277.4	4.47	0.0436	
H – 4 → L + 3	π(hpb) → π*(hpb)	276.8	4.48	0.0437	
H – 2 → L + 4	π(hpb)/d → π*(PPh$_3$)	272.1	4.56	0.0318	
H → L + 8	d/π(hpb) → π*(p-tol)				
H → L + 13	d/π(hpb) → π*(hpb)				
H – 7 → L + 2	π(PPh$_3$)/π(hpb) → π*(hpb)	265.6	4.67	0.0347	
H → L + 9	d/π(hpb) → π*(hpb)				
H – 9 → L + 3	π(PPh$_3$) → π*(hpb)	248.6	4.99	0.0587	201.6 (6.15) 35500
H – 9 → L + 3	π(PPh$_3$) → π*(hpb)	248.0	5.00	0.0600	
H – 16 → L + 1	π(hpb) → d/π*(p-tol)/π*(hpbi)	245.8	5.04	0.0540	
H → L + 15	d/π(hpb) → π*(hpb)	244.5	5.07	0.0385	
H → L + 16	d/π(hpb) → π*(hpb)	242.7	5.11	0.0359	
H – 3 → L + 6	π(hpb)/π(p-tol) → π*(PPh$_3$)	239.7	5.17	0.0612	

ε – molar absorption coefficient [dm^3 mol^{-1} cm^{-1}]; *f* – oscillator strength; H – highest occupied molecular orbital; L – lowest unoccupied molecular orbital.

of the spectrum, only transitions with oscillator strengths larger than 0.030 are listed in Tables 10 and 11. The assignment of the calculated orbital excitations to the experimental bands was based on an overview of the contour plots and relative energy to the occupied and unoccupied orbitals involved in the electronic transitions.

4.8. Electronic spectrum of **1**

The longest wavelength experimental band of **1** at 731.4 nm originates in the HOMO → LUMO and HOMO → LUMO + 1 transitions. As it can be seen from the Fig. 5, the HOMO is composed of p$_\pi$ chloride orbitals and d_{xy} rhenium atomic orbital, the LUMO and LUMO + 1 are delocalized on central ion and π-anti-bonding orbitals of the 4-methylphenylimido ligand with small contribution of π-anti-bonding orbitals of the *hpb*$^-$. Accordingly, the transition at 731.4 nm can be seen as a delocalized MLLCT (*Metal–Ligand-to-Ligand CT*) transition. On the other hand, considering that the molecular orbitals involved in the electronic transitions assigned to the longest wavelength experimental band comprise mainly rhenium 5d atomic orbitals, the HOMO → LUMO and HOMO → LUMO + 1 transitions may be ascribed as transitions of d → d character. The longest wavelength experimental band of **2** is blue shifted and more intense in comparison with **1** (see Section 2).

The transitions assigned to the experimental bands at 323.1 and 294.7 nm can be seen as mixed π(Cl)/π(p-tol)/π(PPh$_3$)/π(hpb) → Re (*Ligand–Metal Charge Transfer*; *LMCT*) and π(Cl)/π(p-tol)/π(PPh$_3$)/π(hpb) → π*(p-tol)/π*(hpb) (*Ligand–Ligand Charge Transfer*; *LLCT*) transitions. The absorption band at 215.9 nm is attributed to the *Ligand–Ligand Charge Transfer* and interligand (*IL*) transitions.

4.9. Electronic spectrum of **3**

Likewise for **1**, the longest wavelength experimental band of **3** may be attributed to the transition of d → d character or may be seen as a delocalized MLLCT (*Metal–Ligand-to-Ligand CT*) transitions.

The transitions leading to the experimental band at 330.8 nm can be seen as mixed π(hpbi) → d$_{\mathrm{Re}}$ (*Ligand–Metal Charge Transfer*; *LMCT*), d$_{\mathrm{Re}}$ → π*(p-tol)/π*(hpbi) (*Metal–Ligand Charge Transfer*; *LMCT*) and π(hpbi) → π*(p-tol)/π*(hpbi) (*Ligand–Ligand Charge Transfer*; *LLCT*) transitions. The absorption bands at 296.8 and 201.6 nm result mainly from *Ligand–Ligand Charge Transfer* and interligand (*IL*) transitions.

5. Conclusions

The reactivity of [Re(p-NC$_6$H$_4$CH$_3$)Cl$_3$(PPh$_3$)$_2$] (X = Cl, Br) towards 2-(2-hydroxyphenyl)-1H-benzimidazole has been examined and compared with the related exchange reactions performed with oxocompounds [ReOX$_3$(PPh$_3$)$_2$]. Novel rhenium(V) imidocomplexes *trans*-[Re(p-NC$_6$H$_4$CH$_3$)X$_2$(hpb)(PPh$_3$)] and [Re(p-NC$_6$H$_4$CH$_3$)(hpb)$_2$(PPh$_3$)]X (X = Cl, Br) have been obtained and characterized structurally and spectroscopically. In all of them the *hpb*$^-$ ion is coordinated in a chelate way *via* N- and O-donor atoms, and the PPh$_3$ molecule is *cis*-located in relation to the Re$\equiv$N moiety, which forces the metal nonbonding *d* electrons to lie in the plane perpendicular to the M$\equiv$N bond axis. The X-ray studies and NBO analysis confirm a linear coordination mode of the p-NC$_6$H$_4$CH$_3$ ligand and triple bond between the rhenium and the imido ligand.

Acknowledgements

The GAUSSIAN-03 calculations were carried out in the Wrocław Centre for Networking and Supercomputing, WCSS, Wrocław, Poland, http://www.wcss.wroc.pl, under calculational Grant No. 51/96.

Appendix A. Supplementary data

CCDC 791217, 791218, 791219, and 791220 contain the supplementary crystallographic data for complexes **1**–**4**. These data can be obtained free of charge via http://www.ccdc.cam.ac.uk/conts/retrieving.html, or from the Cambridge Crystallographic Data Centre, 12 Union Road, Cambridge CB2 1EZ, UK; fax: (+44) 1223-336-033; or e-mail: deposit@ccdc.cam.ac.uk.

References

[1] M. Tadokoro, K. Nakasuji, Coord. Chem. Rev. 198 (2000) 205.
[2] Y. Sunatsuki, Y. Motoda, N. Matsumoto, Coord. Chem. Rev. 226 (2002) 199.
[3] R. Rowan, T. Tallon, A.M. Sheahan, R. Curran, M. McCann, K. Kavanagh, M. Devereux, V. McKee, Polyhedron 25 (2006) 1771.
[4] Y.-M. Fu, Y.-H. Zhao, Y.-Q. Lan, Y. Wang, Y.-Q. Qiu, K.-Z. Shao, Z.-M. Su, Inorg. Chem. Commun. 10 (2007) 720.
[5] T. Higa a, M. Moriya, Y. Shimazaki, T. Yajima, F. Tani, S. Karasawa, M. Nakano, Y. Naruta, O. Yamauchi, Inorg. Chim. Acta 360 (2007) 3304.
[6] P. Deschamps, P.P. Kulkarni, M. Gautam-Basak, B. Sarkar, Coord. Chem. Rev. 249 (2005) 895.
[7] O. Szilágyi, K. Ösz, K. Várnagy, D. Sanna, H. Süli-Vargha, I. Sóvágó, G. Micera, Polyhedron 25 (2006) 3173.
[8] K. Várnagy, I. Sóvágó, H. Süli-Vargha, D. Sanna, G. Micera, J. Inorg. Biochem. 81 (2000) 35.
[9] I. Török, P. Surdy, A. Rockenbauer, L. Korecz Jr., G.J.A.A. Koolhaas, T. Gajda, J. Inorg. Biochem. 71 (1998) 7.
[10] K. Ösz, K. Várnagy, H. Süli-Vargha, A. Csámpay, D. Sanna, G. Micera, I. Sóvágó, J. Inorg. Biochem. 98 (2004) 24.
[11] W. Volkert, W.F. Goeckeler, G.J. Ehrhardt, A.R. Ketring, J. Nucl. Med. 32 (1991) 174.
[12] B. Coutinho, D. Dawson, J.R. Dilworth, J.R. Miller, M. Rosser, C.M. Archer, J.D. Kelly, in: M. Nicolini, G. Bandoli, U. Mazzi, S.G. Editoriali (Eds.), Technetium and Rhenium in Chemistry and Nuclear Medicine, vol. 3, Padova, 1995.
[13] B. Machura, M. Wolff, J. Kusz, R. Kruszynski, Polyhedron 28 (2009) 2949.
[14] C.J. Cramer, D.G. Truhlar, Phys. Chem. Chem. Phys. 11 (2009) 10757.
[15] W. Koch, M.C. Holthausen, A Chemist's Guide to Density Functional Theory, Wiley-VCH, 2000.
[16] J. Chatt, J.D. Garforth, N.P. Johnson, G.A. Rowe, J. Chem. Soc. (1964) 1012.
[17] CRYSALIS RED, Oxford Diffraction Ltd., Version 1.171.33.46, 2009.
[18] G.M. Sheldrick, Acta Crystallogr., Sect. A 64 (2008) 112.
[19] Gaussian 03, Revision D.01, M.J. Frisch, G.W. Trucks, H.B. Schlegel, G.E. Scuseria, M.A. Robb, J.R. Cheeseman, J.A. Montgomery, Jr., T. Vreven, K.N. Kudin, J.C. Burant, J.M. Millam, S.S. Iyengar, J. Tomasi, V. Barone, B. Mennucci, M. Cossi, G. Scalmani, N. Rega, G.A. Petersson, H. Nakatsuji, M. Hada, M. Ehara, K. Toyota, R. Fukuda, J. Hasegawa, M. Ishida, T. Nakajima, Y. Honda, O. Kitao, H. Nakai, M. Klene, X. Li, J.E. Knox, H.P. Hratchian, J.B. Cross, V. Bakken, C. Adamo, J. Jaramillo, R. Gomperts, R.E. Stratmann, O. Yazyev, A.J. Austin, R. Cammi, C. Pomelli, J.W. Ochterski, P.Y. Ayala, K. Morokuma, G.A. Voth, P. Salvador, J.J. Dannenberg, V.G. Zakrzewski, S. Dapprich, A.D. Daniels, M.C. Strain, O. Farkas, D.K. Malick, A.D. Rabuck, K. Raghavachari, J.B. Foresman, J.V. Ortiz, Q. Cui, A.G. Baboul, S. Clifford, J. Cioslowski, B.B. Stefanov, G. Liu, A. Liashenko, P. Piskorz, I. Komaromi, R.L. Martin, D.J. Fox, T. Keith, M.A. Al-Laham, C.Y. Peng, A. Nanayakkara, M. Challacombe, P.M.W. Gill, B. Johnson, W. Chen, M.W. Wong, C. Gonzalez, J.A. Pople, Gaussian, Inc., Wallingford CT, 2004.
[20] A.D. Becke, J. Chem. Phys. 98 (1993) 5648.
[21] C. Lee, W. Yang, R.G. Parr, Phys. Rev. B 37 (1988) 785.
[22] P.J. Hay, W.R. Wadt, J. Chem. Phys. 82 (1985) 299.
[23] K. Eichkorn, F. Weigend, O. Treutler, R. Ahlrichs, Theor. Chem. Acc. 97 (1997) 119.
[24] W.J. Hehre, R. Ditchfield, J.A. Pople, J. Chem. Phys. 56 (1972) 2257.
[25] P.C. Hariharan, J.A. Pople, Theor. Chim. Acta 28 (1973) 213.
[26] M.M. Francl, W.J. Petro, W.J. Hehre, J.S. Binkley, M.S. Gordon, D.J. DeFrees, J.A. Pople, J. Chem. Phys. 77 (1982) 3654.
[27] T. Clark, J. Chandrasekhar, P.V.R. Schleyer, J. Comput. Chem. 4 (1983) 294.
[28] R. Krishnam, J.S. Binkley, R. Seeger, J.A. Pople, J. Chem. Phys. 72 (1980) 650.
[29] P.M.W. Gill, B.G. Johnson, J.A. Pople, M.J. Frisch, Chem. Phys. Lett. 197 (1992) 499.
[30] M.E. Casida, in: J.M. Seminario (Ed.), Recent Developments and Applications in Modern Density Functional Theory, Theoretical and Computational Chemistry, vol. 4, Elsevier, Amsterdam, 1996.
[31] M.T. Cances, B. Mennucci, J. Tomasi, J. Chem. Phys. 107 (1997) 3032.
[32] M. Cossi, V. Barone, B. Mennucci, J. Tomasi, Chem. Phys. Lett. 286 (1998) 253.
[33] B. Mennucci, J. Tomasi, J. Chem. Phys. 106 (1997) 5151.
[34] M. Cossi, G. Scalmani, N. Rega, V. Barone, J. Chem. Phys. 117 (2002) 43.
[35] E.D. Glendening, A.E. Reed, J.E. Carpenter, F. Weinhold, NBO Version 3.1.
[36] B. Machura, R. Kruszynski, Polyhedron 26 (2007) 3686.
[37] B. Machura, J. Kusz, Polyhedron 27 (2008) 187.
[38] B. Machura, R. Kruszynski, J. Kusz, Polyhedron 27 (2008) 1679.
[39] A. Sachse, N.C. Mösch-Zanetti, G. Lyashenko, J.W. Wielandt, K. Most, J. Magull, F. Dall'Antonia, A. Pal, R. Herbst-Irmer, Inorg. Chem. 46 (2007) 7126.
[40] R. Rossi, A. Marchi, A. Duatti, L. Magon, U. Casellato, R. Graziani, G. Polizzotti, Inorg. Chim. Acta 90 (1984) 121.
[41] V.M. Bereau, S.I. Khan, M.M. Abu-Omar, Inorg. Chem. 40 (2001) 6767.
[42] K. Nakamoto, Infrared and Raman Spectra of Inorganic and Coordination Compounds, fourth ed., Wiley-Interscience, New York, 1986.
[43] L. Wei, J. Zubieta, J.W. Babich, Inorg. Chem. 43 (2004) 6445.
[44] G. Bandoli, T.I.A. Gerber, J. Perils, J.G.H. du Preez, Inorg. Chim. Acta 278 (1998) 96.
[45] I. Booysen, T.I.A. Gerber, E. Hosten, P. Mayer, J. Coord. Chem. 60 (2007) 1749.
[46] J.B. Arterburn, K.V. Rao, D.M. Goreham, M.V. Valenzuela, M.S. Holguin, K.A. Hall, K.C. Ott, J.C. Bryan, Organometallics 19 (2000) 1789.
[47] G. Bandoli, A. Dolmella, T.I.A. Gerber, J. Perils, J.G.H. du Preez, Bull. Chem. Soc. Ethiop. 16 (2002) 149.
[48] T.I.A. Gerber, D.G. Luzipo, P. Mayer, J. Coord. Chem. 59 (2006) 1515.
[49] J.B. Arterburn, I.M. Fogarty, K.A. Hall, K.C. Ott, J.C. Bryan, Angew. Chem., Int. Ed. 35 (1996) 2877.
[50] B. Machura, R. Kruszynski, M. Jaworska, Polyhedron 24 (2005) 1454.
[51] G.A. Jeffrey, W. Saenger, Hydrogen Bonding in Biological Structures, Springer Verlag, 1994.
[52] G.R. Desiraju, T. Steiner, The Weak Hydrogen Bond in Structural Chemistry and Biology, Oxford University Press, 1999.
[53] S.R. Flechter, A.C. Skapski, J. Chem. Soc., Dalton Trans. (1972) 1073.
[54] F.H. Allen, Acta Crystallogr., Sect. B 58 (2002) 380.
[55] E. Reed, L.A. Curtiss, F. Weinhold, Chem. Rev. 88 (1988) 899.
[56] M.L. Kuznetsov, A.J.L. Pombeiro, J. Chem. Soc., Dalton Trans. (2003) 738.